

The *Drosophila* pheromone cVA activates a sexually dimorphic neural circuit

Sandeep Robert Datta^{1*}, Maria Luisa Vasconcelos^{1*}, Vanessa Ruta¹, Sean Luo¹, Allan Wong^{1,2}, Ebru Demir³, Jorge Flores¹, Karen Balonze¹, Barry J. Dickson³ & Richard Axel¹

Courtship is an innate sexually dimorphic behaviour that can be observed in naive animals without previous learning or experience, suggesting that the neural circuits that mediate this behaviour are developmentally programmed¹. In *Drosophila*, courtship involves a complex yet stereotyped array of dimorphic behaviours that are regulated by Fru^M, a male-specific isoform of the *fruitless* gene^{2–5}. Fru^M is expressed in about 2,000 neurons in the fly brain, including three subpopulations of olfactory sensory neurons and projection neurons (PNs). One set of Fru⁺ olfactory neurons expresses the odorant receptor Or67d and responds to the male-specific pheromone *cis*-vaccenyl acetate (cVA)^{6–10}. These neurons converge on the DA1 glomerulus in the antennal lobe. In males, activation of Or67d⁺ neurons by cVA inhibits courtship of other males, whereas in females their activation promotes receptivity to other males⁷. These observations pose the question of how a single pheromone acting through the same set of sensory neurons can elicit different behaviours in male and female flies. Anatomical or

functional dimorphisms in this neural circuit might be responsible for the dimorphic behaviour. We therefore developed a neural tracing procedure that employs two-photon laser scanning microscopy to activate the photoactivatable green fluorescent protein¹¹. Here we show, using this technique, that the projections from the DA1 glomerulus to the protocerebrum are sexually dimorphic. We observe a male-specific axonal arbor in the lateral horn whose elaboration requires the expression of the transcription factor Fru^M in DA1 projection neurons and other Fru⁺ cells. The observation that cVA activates a sexually dimorphic circuit in the protocerebrum suggests a mechanism by which a single pheromone can elicit different behaviours in males and in females.

In initial experiments, we expressed photoactivatable green fluorescent protein (PA-GFP) in flies in which the GAL4 enhancer-trap *GHI46* (ref. 12) drives the expression of *UAS-PA-GFP* in 60% of the PNs that innervate most glomeruli in the antennal lobe (Fig. 1a, b). PA-GFP exhibits low-level fluorescence, sufficient to identify

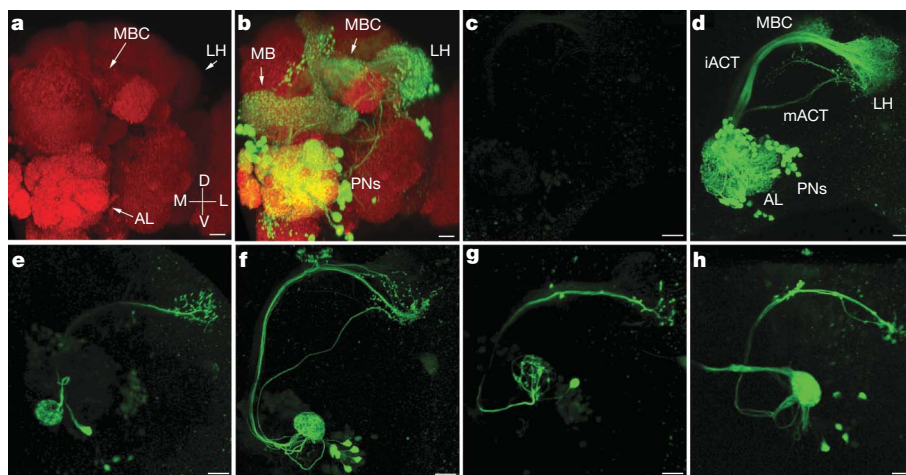


Figure 1 | Tracing populations, subpopulations and single neurons in the *Drosophila* olfactory system. **a**, Z projection of a confocal image of a *Drosophila* brain (*GHI46; UAS-PA-GFP*) stained with the nc82 antibody (red) reveals neuropil, and highlights structures in the olfactory system including the antennal lobe (AL; note individual glomeruli within the lobe), the lateral horn (LH) and the mushroom body calyx (MBC). D, dorsal; V, ventral; M, medial; L, lateral. **b**, Z projection of a confocal image of the same brain in **a** stained with anti-GFP antibodies (green) reveals PA-GFP expression under the control of *GHI46* in projection neurons (lateral PN group indicated by PN label) and intrinsic neurons that innervate the mushroom body (MB). **c**, **d**, Z projections of two-photon laser scanning microscope imaging of live fly brains

expressing PA-GFP under control of the *GHI46* driver before (**c**) and after (**d**) photoconversion reveals PN cell bodies and projections from the antennal lobe to the mushroom body and lateral horn. mACT, medial antennocerebral tract; iACT, inner antennocerebral tract. **e**, **f**, Photoconversion of a single glomerulus VM3 (**e**) or DA1 (**f**) in the live fly brain with the *GHI46* driver. **g**, Photoconversion of a single *GHI46* DA1 PN. **h**, Photoconversion of the DA1 glomerulus in flies expressing PA-GFP under the control of the *Fru* P1 promoter. Note that *GHI46* labels six lateral neurons that project through the iACT and one or two ventral PNs that project through the mACT, whereas *fru*^{GAL4} labels only six lateral neurons that project through the iACT (see Supplementary Fig. 4). All images are oriented similarly to **a**. Scale bars, 10 μ m.

¹Department of Biochemistry and Molecular Biophysics and Howard Hughes Medical Institute, College of Physicians and Surgeons, Columbia University, New York, New York 10032, USA. ²Division of Biology 216-76 and Howard Hughes Medical Institute, California Institute of Technology, Pasadena, California 91125, USA. ³Research Institute of Molecular Pathology (IMP), Dr Bohr-gasse 7, A-1030 Vienna, Austria.

*These authors contributed equally to this work.

individual glomeruli, that is enhanced 100-fold after photoconversion with high-energy light. We photoactivated the PA-GFP with a two-photon laser scanning microscope to localize 710-nm light with submicrometre three-dimensional precision. Photoactivation of the antennal lobe neuropil, encompassing all glomeruli, results in intense labelling of the dendritic arbors of *GHI46* PNs. Diffusion of PA-GFP from the illuminated dendritic arbors allowed us to also reveal the cell bodies and axonal projections of the multiple *GHI46* PNs (Fig. 1c, d). Photoactivation of individual glomeruli (VM3 and DA1) reveals the dendritic arbors, cell bodies and projections of the subpopulation of *GHI46* PNs that innervate a single glomerulus (Fig. 1e, f).

We then devised an approach to allow the tracing of individual PNs that innervate identified glomeruli. We exposed the DA1 glomerulus to low levels of photoconverting light and then rapidly imaged the antennal lobe to identify the PN cell bodies that show modest increases in fluorescence intensity. Under these limiting conditions of photoactivation, diffusion of PA-GFP into axonal projections was not observed. We next strongly photoactivated a single weakly labeled PN cell body at higher light intensity to reveal the axonal projections of an individual PN that innervates the DA1 glomerulus (Fig. 1g). Thus, two-photon laser scanning microscope-mediated activation of PA-GFP provides sufficient spatial resolution and photoconversion energy to reveal the neuronal processes of defined neuronal populations as well as individual neurons in the fly brain.

The development of a combined genetic and optical neural tracing method permitted us to compare the topography of projections from Fru^+ PNs that innervate the cVA-responsive DA1 glomerulus in male and female flies. Flies in which *GAL4* is expressed under the control of the P1 *fruitless* promoter responsible for generating Fru^M (*fru^{GAL4}*)^{2,3} were crossed with flies harbouring the *UAS-PA-GFP* transgene. P1 transcripts from the modified *fru^{GAL4}* allele do not undergo the sexually dimorphic splicing observed for the wild-type *fru* allele, and they therefore allow us to mark Fru^+ cells in both sexes^{2,3}. Unilateral photoactivation of the fly brain reveals many Fru^+ cells, including neurons in the antennal lobe (Supplementary Fig. 1). Specific photoactivation of the DA1 glomerulus reveals six Fru^+ PNs in both male and female flies (Fig. 1h and Supplementary Fig. 4; 6.23 ± 0.13 in females, 6.27 ± 0.14 in males) that innervate this glomerulus. The cell bodies of these neurons reside in the lateral PN cluster, not the dorsal cluster as previously suggested³.

It is possible that the sex-specific behavioural responses to cVA result from different functional responses of the DA1 glomerulus in the two sexes despite there being no apparent difference in the number or location of Fru^+ DA1 PNs. We therefore expressed the Ca^{2+} -sensitive fluorescent protein GCaMP¹³ in Fru^+ neurons and used two-photon imaging to examine increases in Ca^{2+} in the DA1 glomerulus in response to cVA. We detected large increases in Ca^{2+} within the DA1 glomerulus by two-photon imaging after exposure of an intact, behaving fly to cVA (Fig. 2a; see Methods). However, we did not observe any differences between male and female responses over a broad range of cVA concentrations.

These imaging experiments report local changes in the concentration of Ca^{2+} in both the presynaptic and postsynaptic compartments, because both Or67d-expressing neurons and DA1 PNs are Fru^+ (refs 3,4,8,9). We therefore examined whether the electrophysiological properties of Fru^+ DA1 PNs were sexually dimorphic. We photoactivated the DA1 glomerulus to identify Fru^+ DA1 PNs and used the enhanced fluorescence to guide a patch electrode to the cell bodies (Fig. 2b). We recorded from Fru^+ DA1 PNs in the loose patch configuration in an intact fly preparation and noted no significant difference in the spike frequency or response kinetics between males and females when tested at several concentrations of cVA (Fig. 2c, d). These responses are comparable to those previously observed in whole-cell recordings of female DA1 PNs¹⁴. This result demonstrates that male and female DA1 PNs show similar electrophysiological responses to cVA despite the previously noted dimorphism in the size of the DA1 glomerulus^{3,4,15}.

We next examined the projection patterns of Fru^+ DA1 PNs in the two sexes. Photoconversion of the DA1 glomerulus allowed us to reveal the projection patterns of the population of DA1 PNs in the lateral horn in living brains. Despite significant similarity in the axonal arbors of DA1 PNs in males and females (Fig. 3a), we observed an increase in the density of ventral axonal branches in the male (Fig. 3a, arrowhead). Quantification of differences in branch patterns in multiple individual male and female flies was hampered by variations in the orientation of the live brain during microscopy. We therefore altered our approach to employ fixed brains stained with the antibody nc82 to label the synaptic neuropil of the lateral horn. We used an image registration algorithm (see Methods) to first 'warp' the nc82 channel of individual brains onto a reference brain¹⁶ and then map the PA-GFP fluorescence onto this reference brain (Fig. 3b). The registration error averaged less than $2 \mu\text{m}$ in any dimension when measured at the neuropil edge (Supplementary Fig. 2). We observed that the projections from the DA1 glomerulus target the anterior ventromedial region of the LH. The projection pattern is triskelion-shaped, with ventral, lateral and dorsal branches. Fru^+ DA1 projections from males have additional axonal branches that extend ventromedially (Fig. 3c). Superposition of the DA1 projections taken from ten male and ten female flies confirms this observation (Fig. 3d), indicating that information carried by Fru^+ DA1 PNs is differentially segregated in the lateral horn of the two sexes. As a control we performed a similar analysis of the PN projections from the Fru^- glomerulus VM3, which responds to alcohols and acetates^{8,9,17}. Superposition of the projections from VM3 reveals no consistent differences in the pattern of axonal projections in the lateral horn between the two sexes (Fig. 3e, f). These observations show that our image alignment procedure does not introduce sex-specific biases in projection patterns and that the dimorphic

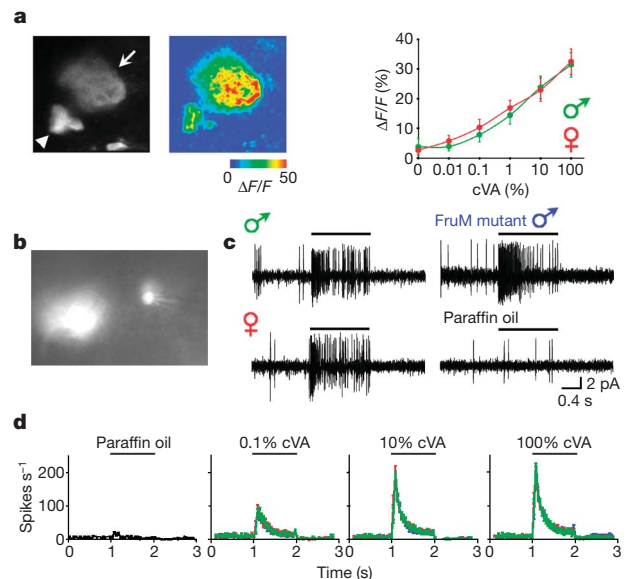


Figure 2 | Functional characterization of the DA1 glomerulus and Fru^+ DA1 PNs. **a**, Two-photon laser scanning microscope imaging of background fluorescence (left) and pseudocoloured maximal response (middle) of the DA1 glomerulus (arrow) and PNs (arrowhead) to cVA in a fly expressing the fluorescent Ca^{2+} reporter GCaMP in Fru^+ cells. Peak average glomerular responses of male (green) and female (red) flies after a 1-s exposure to cVA at the indicated doses (left, $n = 8$ per sex; error bars indicate s.e.m.). **b**, Epifluorescence image of a patch pipette targeting a Fru^+ DA1 PN after photoconversion of the DA1 glomerulus. **c**, **d**, Single traces (**c**) and peristimulus time histograms (**d**) (error bars indicate s.e.m.; $n = 6$ per genotype) of loose patch recordings of male, female and *fru* mutant male flies (colours indicated in **c**) before and after a 1-s exposure to cVA at the doses indicated.

projection patterns we observe for the Fru^+ glomerulus DA1 are not a general feature of projections from all glomeruli.

The anatomical dimorphism observed at the level of the population of axons is also shown by the axons of single identified neurons. Tracing individual Fru^+ DA1 neurons after warping revealed that the ventral axonal branches of male PNs define a male-specific region of protocerebral space (about $600 \mu\text{m}^3$; Figs 4 and 5a, and Supplementary Fig. 3). Each individual male in our data set sends at least one axon branch into this area. This area seems to partly overlap a region of neuropil in the lateral horn that was recently shown to be larger in male flies than in female flies¹⁶. In addition, the total density of ventrally oriented axonal branches is significantly greater in males than in females (Fig. 5a). In contrast, the total innervation of the dorsal axonal arbor showed no statistically significant differences between sexes (Fig. 5a). We were unable to identify a similar female-specific area, although there are several smaller areas (particularly laterally) that appear to have an increased

density of female axons. The data from single-axon tracing, along with our observations from populations of DA1 neurons, indicate that DA1 PN projections are sexually dimorphic.

Fru mutant males court other males with high frequency^{2,3}. If the male-specific arbor contributes to the dimorphic behavioural response, we expect that the DA1 PN projection patterns will be regulated by the *fruitless* gene. We therefore made visible the axonal projections of single DA1 PNs in *fru* mutant males, and observed that DA1 PNs lack the characteristic male-specific axonal branches and exhibit a branching pattern more characteristic of wild-type females. However, the feminization is not complete in that the male-specific ventral axonal branches are significantly reduced but not completely eliminated in *fru* mutant males (Figs 4 and 5a). Thus, the male pattern of projections of Fru^+ DA1 PNs requires the male-specific isoform of *fru*, Fru^M .

We also show that the ectopic expression of Fru^M in females masculinizes the axonal arbor of their DA1 PNs. Projections of single Fru^+ DA1 PNs in female flies that express Fru^M (*fru^{GAL4}/fru^{UAS-Fru^M}*; see Methods) exhibit a striking increase in axonal projections to the ventral male-enhanced area (Fig. 4). Quantitative analysis of these

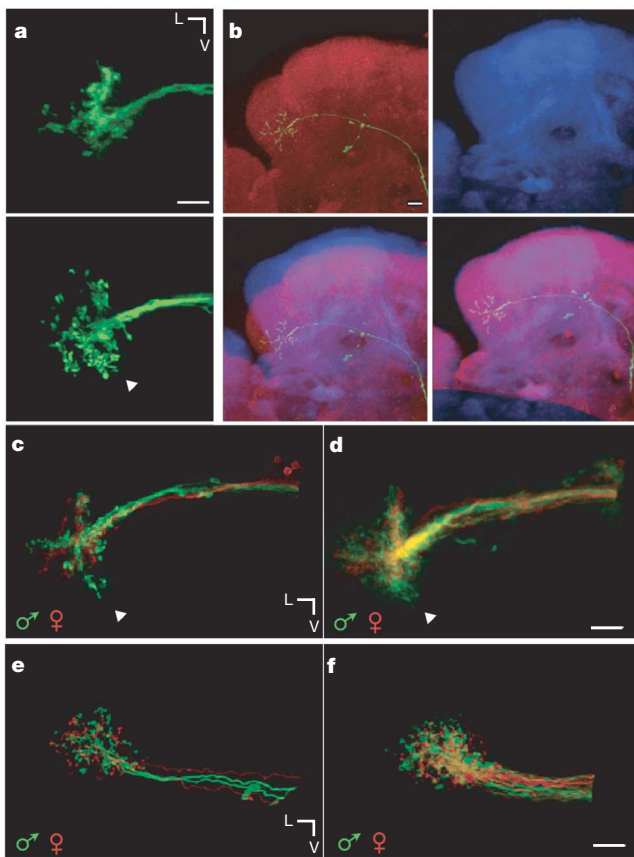


Figure 3 | Tracing and registration of DA1 glomerular projections reveals sexually dimorphic projections in the lateral horn. **a**, Z projection of two-photon laser scanning microscope images of the lateral horns of live female (top) and male (bottom) fly brains after photoconversion of the DA1 glomerulus. Apparent increased ventral male density is indicated by an arrowhead. **b**, Top left: two-channel brain image of a single neuron labelled by photoconversion (green) before immunostaining with nc82 antibody (red) to mark neuropil. Top right: reference brain generated by averaging ten male and ten female nc82 channels. Bottom left: superposition of these images before warping. Bottom right: superposition of these images after warping. **c**, Superposition of male (green) and female (red) projections after photoconversion of all Fru^+ DA1 PNs in single flies reveals a ventral region of sexual dimorphism (arrowhead). **d**, Superposition of ten male and ten female DA1 projection patterns after photoconversion of all Fru^+ DA1 PNs. **e**, Superposition of photoconverted male (green) and female (red) projections from the VM3 glomerulus in single flies, similar to **c**. Note that VM3 typically labels two PNs, which travel in independent pathways through the iACT. **f**, Image similar to **d**, with superposition of seven male and seven female photoconverted VM3 projection patterns. Scale bars, $10 \mu\text{m}$.

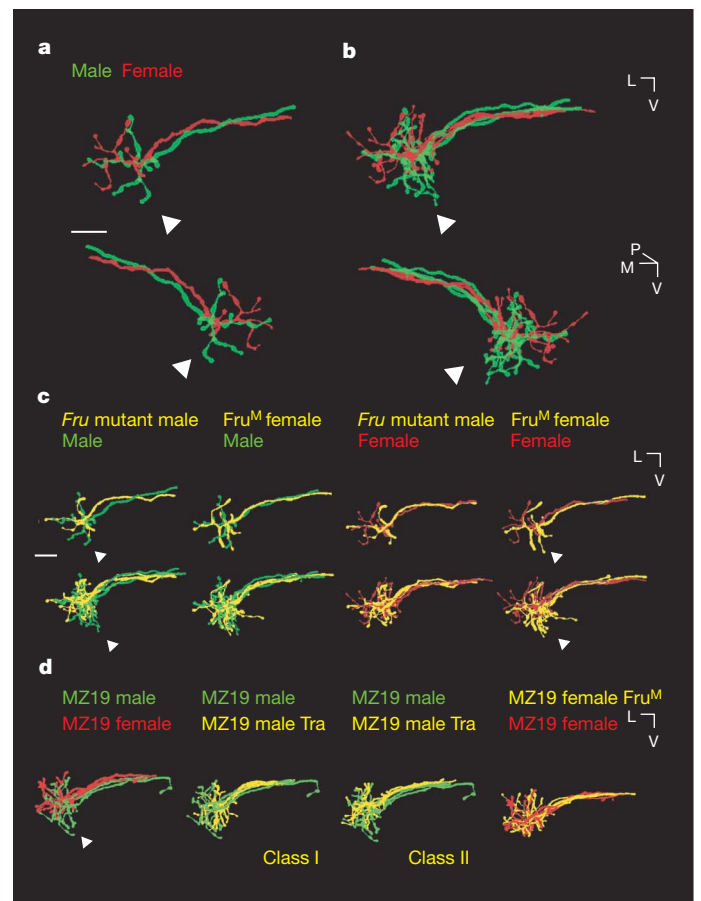


Figure 4 | Fru^M controls sexually dimorphic pheromone response circuitry. **a**, Superposition of traces of single Fru^+ DA1 PNs in Z projection (top) and after rotation about 120° about the Z axis (lower) projections. Genotypes (male, female) are coloured as indicated. Lateral and ventral correspond to x and y imaging axes, respectively; posterior corresponds to the z axis. **b**, Images as in **a** including three neurons overlaid as in **a** and **b** in Z projection with genotypes (male, female, *fru* mutant male and female expressing Fru^M) in the colours indicated. Arrowheads indicate the ventral region that shows enhanced male innervation. **c**, Superposition of traces of three MZ19 DA1 PNs in Z projection, with genotypes (MZ19 male, MZ19 female, MZ19 male expressing Tra, MZ19 female expressing Fru^M) in the colours indicated. Enhanced ventral male innervation is indicated by an arrowhead. Class I PNs are male neurons expressing Tra that have masculine arbors, whereas class II PNs have feminine arbors (see Supplementary Fig. 5). Scale bar, $10 \mu\text{m}$.

branches reveals that expression of Fru^M in females renders their ventral axon branch pattern statistically indistinguishable from that of males (Fig. 5). The innervation patterns of individual neurons are sufficient for a computational discrimination algorithm to effectively distinguish individual females from Fru^M-expressing females with 100% accuracy, and individual males from *fru* mutant males with more than 91% accuracy (Supplementary Fig. 3). Thus, analysis of the PN projections of both single defined neurons and populations of neurons reveal that Fru⁺ DA1 PNs project to different regions of the protocerebrum in male and female flies. Moreover, this anatomical dimorphism in the neural circuit is controlled by the dimorphic transcription factor, Fru^M.

We next examined whether the formation of the male-specific arbor requires the action of Fru^M in DA1 projection neurons. The enhancer-trap *MZ19* (refs 18,19) drives the expression of GAL4 in six DA1 PNs, about ten additional PNs that innervate two Fru⁻ glomeruli, and 25 extrinsic neurons of the mushroom body (Supplementary Fig. 4a). Flies harbouring *fru*^{GAL4}, *MZ19* or *MZ19;fru*^{GAL4} all reveal expression of PA-GFP in six DA1 PNs (Supplementary

Fig. 4b). This suggests that the six lateral DA1 neurons labelled by the *MZ19* and *fru*^{GAL4} lines are identical. In accord with this observation, male and female DA1 neurons in *MZ19* flies have a sexually dimorphic pattern of projections that closely resembles the dimorphic branching observed for Fru⁺ DA1 PNs (Figs 4d and 5b, and Supplementary Figs 4a and 5). We therefore eliminated Fru^M expression in male *MZ19* neurons by expression of Tra, which directs the female-specific splicing of *fruitless* transcripts^{20–22}. Genetic feminization of male DA1 PNs in *MZ19/UAS-tra* flies results in two anatomical classes of DA1 projection neurons. Half of the genetically feminized DA1 PNs show a reduction in the male-specific arbor and closely resemble male DA1 projection neurons defective for Fru^M. The remaining genetically feminized neurons exhibit the wild-type male-specific branching patterns (Fig. 4d and Supplementary Fig. 5). Within a single male *MZ19/UAS-tra* fly, neurons of both anatomical classes were observed. These data suggest that Fru^M is required in DA1 PNs to generate a male-specific projection pattern, but its action in this genetic context is partly penetrant.

We have also examined whether the expression of Fru^M in female DA1 PNs masculinizes the DA1 axon arbor. DA1 PNs in female *MZ19; fru*^{UAS-Fru^M} flies do not significantly innervate the male-specific area, although most send minor branches into the ventral region of the lateral horn (Figs 4d and 5b, and Supplementary Fig. 5). This is in contrast with observations with *fru*^{GAL4}/*fru*^{UAS-Fru^M} strains that exhibit a transformation of the female DA1 PN branching pattern into a complete male-specific arbor (Figs 4 and 5a). Taken together, these results suggest that Fru^M is required in both DA1 PNs and in other Fru⁺ neurons to generate the male-specific pattern of ventral axon arborization in the lateral horn.

In *Drosophila*, courtship behaviour is governed by pheromonal excitation of peripheral olfactory pathways that ultimately activate behavioural circuits in higher brain centres. One pheromone elaborated by the male, cVA, suppresses male–male courtship but in females enhances receptivity to courting males⁷. cVA activates the DA1 glomerulus, which is innervated by PNs^{3,4} that have sexually dimorphic projections in the lateral horn. This dimorphic circuit is under control of the transcription factor Fru^M, a male-specific isoform of *fruitless*. Moreover, the dimorphism in this circuit correlates with behaviour. In males mutant for Fru^M, cVA no longer suppresses male–male courtship and males exhibit a feminized pattern of DA1 projections. In females that express Fru^M, DA1 PNs exhibit a male pattern of axonal arbors in the lateral horn, and these females show reduced sexual receptivity (M.L.V. and R.A., unpublished observations). These observations are in accord with a mechanism in which the anatomical differences we observe in Fru⁺ DA1 projection neurons contribute to the distinct behaviours elicited by cVA in the two sexes. In *Drosophila*, dimorphism in the Fru⁺ SP2 (ref. 3) and mAL neurons²³ has been observed, but the behavioural function of these circuits is unknown.

The anatomical dimorphism we observe may be translated into a behavioural dimorphism if the connections between DA1 PNs and third-order neurons differ between the sexes. Third-order neurons whose dendrites innervate the ventral lateral horn may either receive greater input from male PNs or may restrict their synapses to the male-specific region of the DA1 axon arbor. The relatively small size of the male-specific arbor, about the volume of a glomerulus, implies a precision of connectivity in higher processing centres in the fly brain. The stereotyped and local precision of synaptic connections is an organizing principle in the antennal lobe and may be a common feature of invertebrate nervous systems.

Characterization of specific neural circuits that may mediate behaviour, as we describe here for the pheromone-responsive DA1 pathway, requires the development of tracing approaches that label defined populations of neurons. The distinction between genetic approaches—including MARCM²⁴, Flp-Out^{25,26} and PA-GFP-based tracing—and the histological approaches of Golgi and Cajal²⁷ 100 years ago is the ability to use genetic markers to identify partners

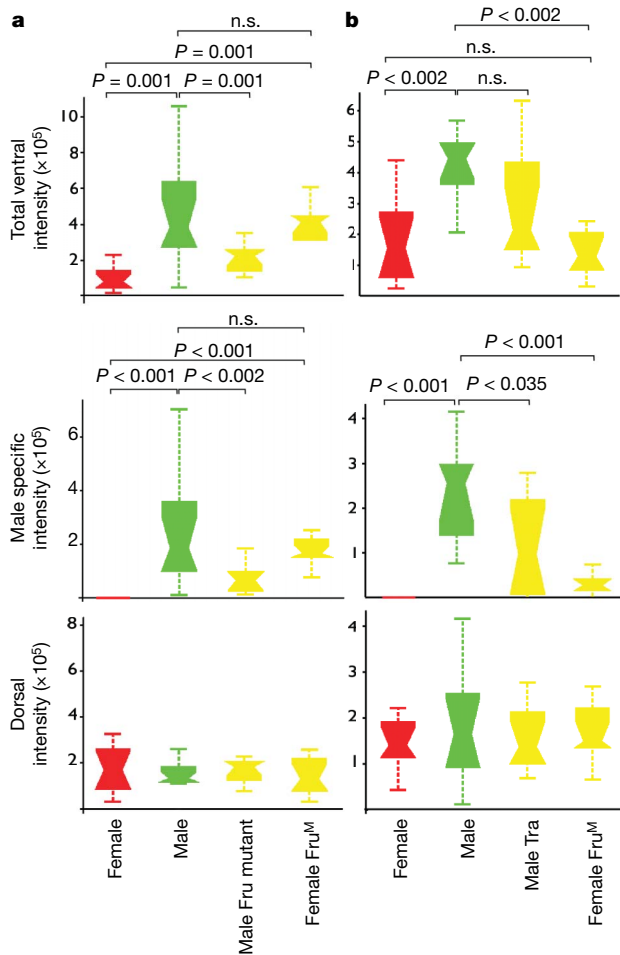


Figure 5 | Quantitative analysis of ventral male-enhanced region. **a**, Box plot of ventrally oriented branch density, male-specific branch density and dorsal branch density of individual traced *fru*^{GAL4} neurons (see Supplementary Fig. 3 for a graphical illustration of the quantified regions) in arbitrary units, with genotypes as indicated. The median is given by the box-plot waist, the top and bottom of boxes denote the 25th and 75th centiles, and range bars denote the largest and smallest data point within 2 s.d. of the mean; outliers greater than 1.5-fold the interquartile range are not shown ($n = 12$ males, $n = 10$ females, $n = 10$ females expressing Fru^M, $n = 9$ *fru* mutant males). **b**, Analysis similar to that in **a** for *MZ19* males ($n = 10$), *MZ19* females ($n = 10$), *MZ19* males expressing Tra ($n = 10$) and *MZ19* females expressing Fru^M ($n = 9$). *P* values in both panels for relevant comparisons are shown by Wilcoxon pairwise rank sum test.

in the neural circuit more precisely. The targeted illumination of PA-GFP permits non-random, optically guided labelling of individual neurons from either anatomically or genetically defined subsets of neurons. Moreover, PA-GFP can be photoactivated in neurons in the living brain and allows electrophysiological recordings of labelled cells. This approach to neural tracing and recording in a defined circuit can be readily adapted to other brain regions in both the fly and mouse.

METHODS SUMMARY

In brief, PA-GFP-based neuronal tracing was performed with *UAS-PA-GFP* flies that were crossed to driver lines expressing Gal4 in specific subsets of neurons. Photoconversion of PA-GFP and tracing of glomerulus-specific projection neurons was achieved after first revealing PA-GFP background fluorescence at the imaging wavelength (925 nm) by two-photon microscopy with relatively high laser powers. These background images allowed the identification of glomeruli (and the specification of regions of interest within these glomeruli to target for photoconversion) on the basis of anatomical position. Because of unavoidable variability in our preparation, each glomerulus was initially subjected to one to three probe pulses of laser light at the photoconversion wavelength (710 nm) to establish empirically the minimum power (range 5–40 mW) required for the effective photoactivation of PA-GFP; this step prevented excessive photodamage or photobleaching of the PA-GFP. We then pulsed the targeted region with 710-nm light using a protocol that incorporated fixed waiting periods to permit the photoconverted PA-GFP to effectively diffuse out of the targeted area and label connected cell bodies and projections. Single neurons were identified for targeted photoconversion by acquiring an initial background Z-stack before subjecting the brain to any photoconversion, and then applying one to three probe pulses of photoconverting 710-nm light to the glomerulus of interest as described above. A second Z-stack was then acquired, and both Z-stacks were compared using the ImarisXT 3D image rendering software (Bitplane). Projection neurons whose fluorescence intensity was increased as a result of photoconversion of a glomerulus were identified, and their cell bodies were targeted for exposure to 710-nm light as described above.

Detailed descriptions of fly stocks, two-photon microscopy, functional imaging, electrophysiology, image registration, image analysis and discriminator construction and analysis are given in the Supplementary Methods section.

Received 20 December 2007; accepted 8 February 2008.

Published online 27 February 2008.

- Hall, J. C. The mating of a fly. *Science* **264**, 1702–1714 (1994).
- Demir, E. & Dickson, B. J. *fruitless* splicing specifies male courtship behavior in *Drosophila*. *Cell* **121**, 785–794 (2005).
- Stockinger, P. *et al.* Neural circuitry that governs *Drosophila* male courtship behavior. *Cell* **121**, 795–807 (2005).
- Manoli, D. S. *et al.* Male-specific *fruitless* specifies the neural substrates of *Drosophila* courtship behaviour. *Nature* **436**, 395–400 (2005).
- Billeter, J. C. *et al.* Isoform-specific control of male neuronal differentiation and behavior in *Drosophila* by the *fruitless* gene. *Curr. Biol.* **16**, 1063–1076 (2006).
- Clyne, P., Grant, A., O'Connell, R. & Carlson, J. R. Odorant response of individual sensilla on the *Drosophila* antenna. *Invert. Neurosci.* **3**, 127–135 (1997).
- Kurtovic, A., Widmer, A. & Dickson, B. J. A single class of olfactory neurons mediates behavioural responses to a *Drosophila* sex pheromone. *Nature* **446**, 542–546 (2007).

- Couto, A., Alenius, M. & Dickson, B. J. Molecular, anatomical, and functional organization of the *Drosophila* olfactory system. *Curr. Biol.* **15**, 1535–1547 (2005).
- Fishilevich, E. & Vosshall, L. B. Genetic and functional subdivision of the *Drosophila* antennal lobe. *Curr. Biol.* **15**, 1548–1553 (2005).
- Ha, T. S. & Smith, D. P. A pheromone receptor mediates 11-*cis*-vaccenyl acetate-induced responses in *Drosophila*. *J. Neurosci.* **26**, 8727–8733 (2006).
- Patterson, G. H. & Lippincott-Schwartz, J. A photoactivatable GFP for selective photolabeling of proteins and cells. *Science* **297**, 1873–1877 (2002).
- Stocker, R. F., Heimbeck, G., Gendre, N. & de Belle, J. S. Neuroblast ablation in *Drosophila* P[GAL4] lines reveals origins of olfactory interneurons. *J. Neurobiol.* **32**, 443–456 (1997).
- Nakai, J., Ohkura, M. & Imoto, K. A high signal-to-noise Ca²⁺ probe composed of a single green fluorescent protein. *Nature Biotechnol.* **19**, 137–141 (2001).
- Schlieff, M. L. & Wilson, R. I. Olfactory processing and behavior downstream from highly selective receptor neurons. *Nature Neurosci.* **10**, 623–630 (2007).
- Kondoh, Y., Kaneshiro, K. Y., Kimura, K. & Yamamoto, D. Evolution of sexual dimorphism in the olfactory brain of Hawaiian *Drosophila*. *Proc. R. Soc. B* **270**, 1005–1013 (2003).
- Jefferis, G. S. *et al.* Comprehensive maps of *Drosophila* higher olfactory centers: spatially segregated fruit and pheromone representation. *Cell* **128**, 1187–1203 (2007).
- Hallam, E. A. & Carlson, J. R. Coding of odors by a receptor repertoire. *Cell* **125**, 143–160 (2006).
- Ito, K. *et al.* The organization of extrinsic neurons and their implications in the functional roles of the mushroom bodies in *Drosophila melanogaster* Meigen. *Learn. Mem.* **5**, 52–77 (1998).
- Jefferis, G. S. *et al.* Developmental origin of wiring specificity in the olfactory system of *Drosophila*. *Development* **131**, 117–130 (2004).
- Heinrichs, V., Ryner, L. C. & Baker, B. S. Regulation of sex-specific selection of *fruitless* 5' splice sites by transformer and transformer-2. *Mol. Cell. Biol.* **18**, 450–458 (1998).
- Ito, H. *et al.* Sexual orientation in *Drosophila* is altered by the satori mutation in the sex-determination gene *fruitless* that encodes a zinc finger protein with a BTB domain. *Proc. Natl Acad. Sci. USA* **93**, 9687–9692 (1996).
- Ryner, L. C. *et al.* Control of male sexual behavior and sexual orientation in *Drosophila* by the *fruitless* gene. *Cell* **87**, 1079–1089 (1996).
- Kimura, K., Ote, M., Tazawa, T. & Yamamoto, D. *Fruitless* specifies sexually dimorphic neural circuitry in the *Drosophila* brain. *Nature* **438**, 229–233 (2005).
- Lee, T. & Luo, L. Mosaic analysis with a repressible cell marker (MARCM) for *Drosophila* neural development. *Trends Neurosci.* **24**, 251–254 (2001).
- Wong, A. M., Wang, J. W. & Axel, R. Spatial representation of the glomerular map in the *Drosophila* protocerebrum. *Cell* **109**, 229–241 (2002).
- Basler, K. & Struhl, G. Compartment boundaries and the control of *Drosophila* limb pattern by hedgehog protein. *Nature* **368**, 208–214 (1994).
- Cajal, S. R. *Manual de Histologia normal y Tecnica micrografica* (Pascual Aguilar, Valencia, 1889).

Supplementary Information is linked to the online version of the paper at www.nature.com/nature.

Acknowledgements We thank G. Struhl, L. Vosshall, B. Sabatini, B. Bloodgood and members of the Axel laboratory for discussions about the experiments in this manuscript; J. Meier for technical assistance; J. Rafter for assistance in measuring the microscope point-spread function; A. Gerber for assistance with warping techniques; and P. J. Kisloff for assistance in the preparation of this manuscript. Financial support was provided by the Helen Hay Whitney Foundation (S.R.D., V.R.) and the Howard Hughes Medical Institute, the Mathers Foundation and the Gates Foundation (R.A.).

Author Information Reprints and permissions information is available at www.nature.com/reprints. Correspondence and requests for materials should be addressed to R.A. (ra27@columbia.edu).